Adsorption of nitrogen oxides by the moisture-saturated zeolites in gas stream

Jing Yang [a], Ting Ting Zhuang [a], Feng Wei [a], Yu Zhou [a], Yi Cao [a], Zheng Ying Wu [a], Jian Hua Zhu [a,*], Chuan Liu [b]

[a] Key Laboratory of Mesoscopic Chemistry, School of Chemistry and Chemical Engineering, Nanjing University, Nanjing 210093, China
[b] GR&D, British American Tobacco, Waterhouse Way, Southampton SO15 8TL, UK

ARTICLE INFO

ABSTRACT

This investigation examined the instantaneous adsorption of NO_x by moisture-saturated zeolites at ambient temperature. Among the zeolites studied, Faujasite exhibited the highest adsorption capacity owing to its relatively large pore size. Besides, the influence of cation was demonstrated by comparing the adsorption of zeolites with different cation densities (NaX vs. NaY, mesoporous silica MCM-48-like vs. Faujasite) and treatments (ion exchange of NaY with Cu^{2+}). For the adsorption of NO, the effects of gas flow rates and pre-adsorbed hydrocarbons such as benzene, acetaldehyde or 1,3-butadiene were evaluated. It was proven that zeolite could efficiently capture nitrogen oxides in gas stream even it had been saturated by moisture, which will be valuable for the protection of environment and public health.

© 2008 Elsevier B.V. All rights reserved.

1. Introduction

Nitrogen oxides (NO_x) are common air pollutants generated by various combustion processes including cigarette smoke [1–6]. Compared to the extensive research on NO_x reduction in other applications [7], relatively little literature exists on effective NO_x reduction in cigarette smoke and related indoor air. Fresh mainstream cigarette smoke (i.e., smoke exiting the mouth end of the cigarette) contains ca. 100–600 µg NO per cigarette [8,9], and the NO in cigarette smoke is quickly oxidized to NO_2 within few seconds due to the atmospheric oxidation [10]. The combined total of NO and NO_2 comprises more than 90% of the nitrogen oxides in cigarette smoke. The importance of NO_x is linked to the fact that they may react with other compounds in the smoke to generate nitrosamines, propenal, hydrazines, amines, urethane and quinoline [11,12]. NO is also known to participate in free radical reactions [13]. In this work our objective was to conduct preliminary study on the adsorption of NO_2 and NO by zeolite in ambient temperature.

Zeolite is a class of alumino-silicates characterized by ordered microporous structures with acid-basic sites on the surface and energetic field inside the pores [14]. Apart from their applications in chemical industry as adsorbents and catalysts, they can be designed

to trap volatile nitrosamines and NO_x in industrial gas streams [15–17] and cigarette smoke [14,18,19]. However, applying zeolite to adsorb nitrogen oxides in a chemical complex system such as tobacco smoke requires careful consideration on some new challenges. The main challenge is the complexity of the cigarette smoke [11], i.e., a mixture of over 4000 compounds in a dynamic aerosol system. The gas flow velocity under a standard ISO smoking condition (2-s puff duration and 35 ml puff volume) through a cigarette filter is ca. $36\,cm\,s^{-1}$, giving a smoke residence (or contact) time of less than 0.1 s. In addition, the adsorbent needs to maintain its activity in the presence of moisture (typically above ca. 13%) [20], the high level of moisture is particularly challenging as many zeolites have high hydrophilicity [21].

For thermally activated zeolites (i.e., containing little moisture), Xu et al. reported that the adsorption of NO_2 by zeolite with different pore sizes. They found that the amount of NO_x adsorbed increases as the pore size changes from 0.4 to 0.8 nm [19]. Among the zeolites assessed, NaY exhibited a strong ability to adsorb NO_2 owing to its large pore size and pore volume. On the other hand, Faujasite such as zeolite NaY could adsorb ca. 25 wt% of water [21,22]. Our previous work showed that moisture in zeolite had negligible impact on the adsorption of volatile nitrosamines in gas stream [23]. However, the performance and mechanisms by which zeolite interact with NO_x in the presence of moisture is still unclear.

Incorporating metal ions into zeolites can potentially strengthen the electrostatic interaction. For example, copper-containing

* Corresponding author. Tel.: +86 25 83595848; fax: +86 25 83317761.
E-mail address: jhzhu@nju.edu.cn (J.H. Zhu).

Table 1
Relevant parameters for the adsorbents tested

	NaY	NaX	Naβ	Hβ	MCM-48-like	Activated carbon
Ratio of Si/Al	2.86	1.24	14	14	ND	ND
Pore size (nm)	0.74	0.74	0.66×0.67	0.66×0.67	9.2	1.0[a]
Surface area ($m^2\,g^{-1}$)	766	900	543	607	903	1000

ND: aluminum is absent in this adsorbent.

[a] This is a mean diameter.

zeolites have been found to be active in adsorbing NO_x [24,25]. Recently we have demonstrated that copper-containing zeolites enhanced decomposition of volatile nitrosamines [26,27]. In this research, commercial zeolites and their copper-modified analogues have been evaluated for their adsorption on NO_2 and NO under the conditions similar to that in a cigarette filter, i.e., in the presence of moisture together with transient gas flow.

2. Experimental

2.1. Reagents and chemicals

Wenzhou Catalysts Factory and Nanjing Chemistry Factory (China) provided the commercial powder zeolite NaY and NaX, respectively. The activated carbon used in this study was a product of Chemviron Carbon (Belgium, CAS number 7440-44-0). Zeolites Hβ were gifts from BASF [28], and Naβ was obtained by ion exchange from Hβ [29]. The MCM-48-like mesoporous silica was prepared in our laboratory [30]. Table 1 illustrates the relevant parameters of these adsorbents.

Copper was incorporated into NaY through impregnation. This was achieved by dissolving $0.456\,g$ $Cu(NO_3)_2 \cdot 3H_2O$ in $40\,ml$ of distilled water and followed by adding $5\,g$ NaY. The mixture was stirred vigorously and heated up to $353\,K$. The product was dried at $373\,K$ overnight and the solid collected was ground into granulate form (ca. $0.15\,mm$ in diameter) and calcined at $773\,K$ for $6\,h$ in N_2 to convert $Cu(NO_3)_2$ to copper oxide. The resulting sample contained 3% (w/w) CuO and was denoted as 3%CuO/NaY [26]. Different concentrations of $Cu(NO_3)_2$ were prepared using this approach to obtain different loading of copper oxide.

A slightly different approach involved carrying out multiple exchange and conversion procedures. The samples thus prepared were denoted as CuY-n, where n represents the exchange times (1, 2 and 3, etc.). Briefly, $2\,g$ NaY was added into a $0.02\,M$ $Cu(NO_3)_2$ solution at $303\,K$. The mixture was stirred for $24\,h$, washed and filtered, then dried at $373\,K$ overnight before calcined at $773\,K$ in N_2 for $6\,h$. The copper contents were determined by ICP (inductively coupled plasma) to reflect the exchange degree of the zeolite, and the percentage of copper on CuY-1, CuY-2 and CuY-3 samples was 2.51, 6.49 and 7.17%, respectively. Table 1 lists the properties of all the adsorbent samples tested in this work.

The purity of NO_2 and NO was greater than 99% and the mixture of NO/N_2 (v/v, 1/49) was prepared as the adsorbate. Nitrogen with 99.99% purity was used as the carrier gas in both the NO_2-TPD (temperature programmed desorption) and NO adsorption experiments.

2.2. Experimental methods

For the NO_2-TPD experiment, prior to either static or dynamic adsorption test, blank run was carried out to ensure no NO_2 adsorption by the empty Pyrex glass-reactor. Zeolite samples were conditioned at $291\,K$ at 79% relative humidity for $12\,h$ prior to use. $0.1\,g$ of the test sample (20–40 mesh, ca. 0.42–$0.84\,mm$ granules) was added into the glass-reactor ($5\,mm$ diameter and $300\,mm$ long)

to form the adsorption bed, and the length of the bed was between ca. 1.3–$2.0\,cm$.

For static adsorption tests, $10\,ml$ NO_2 ($0.320\,mmol$) was introduced to the reactor at $303\,K$ for $20\,min$. The reactor was then purged by N_2 flow at $30\,ml\,min^{-1}$ for $4\,h$. To completely desorb the NO_2, the reactor was heated to $773\,K$ at $10\,K\,min^{-1}$. A CrO_3 tube was used to oxidize any reduced NO_2 prior to trapping [19], and the desorbed NO_2 was trapped by a solution containing sulfanilamide and N-1-naphthylenediamine dihydrochloride. The desorbed NO_2 was collected every $20\,K$ in the range of 323–$773\,K$ and it absolute amount was detected by photometric measurements [19]. After the temperature reached $773\,K$ and the sample was hold at $773\,K$ for $2\,h$, the desorbed NO_2 was collected and detected by every $10\,min$. A $2.5\,M$ NaOH solution was used to treat the waste gas in order to avoid environment contamination. Finally, the total amount of NO_2 desorbed was got by adding all data collected during the experiment.

For dynamic adsorption tests, the same amount of NO_2 ($0.320\,mmol$) was added in a flow of N_2 carrier gas with a flow rate of $30\,ml\,min^{-1}$ at $303\,K$. The sample in the reactor was purged and desorbed in the same procedures as in the static adsorption tests.

The temperature for instantaneous adsorption tests for NO was kept at $303\,K$. In this case, $0.03\,g$ of zeolites (20–40 mesh, conditioned as before) was used to fill the Pryrex glass-reactor to form ca. 0.5–$0.65\,cm$ long adsorption bed. The NO–N_2 mixture with $2.0\,\mu mol$ of NO and volume ratio of 1:49 was injected through the adsorption bed every $10\,min$ with $30\,ml\,min^{-1}$ N_2 [23]. Each adsorption test lasted for less than $0.3\,s$. The residual NO in the gas flow passed through a CrO_3 tube to be oxidized to NO_2 and the amount of residual NO was collected and detected every $10\,min$ [19]. This transient adsorption was repeated until the amount of residual NO detected in the outlet gas stream closed to that of NO injected into the reactor. The difference between the total amount and the residual amount of NO represented the amount adsorbed by the sample.

3. Results

3.1. NO_2-TPD on zeolites

Table 2 shows the NO_2 adsorption results obtained by TPD on the moisture-saturated zeolites and the other porous materials. This was a static adsorption test conducted at $303\,K$, and the NaY sample exhibited adsorption ability ($373.6\,\mu mol\,g^{-1}$) larger than the activated NaY ($301\,\mu mol\,g^{-1}$) and Naβ ($263.1\,\mu mol\,g^{-1}$). Also, the amount of NO_2 thermally desorbed from NaY was greater than that of Naβ, 59% as oppose to 39%. Among the ordered porous adsorbents tested, however, the largest amount of desorption occurred on NaX (ca. $669\,\mu mol\,g^{-1}$), ca. 1.79 times higher than that of NaY although the two samples had the same pore size. As seen in Table 2, zeolite NaX exhibit a higher desorption of NO_2 (B), the NO desorbed after the temperature reached $773\,K$, than other materials. This difference originates from the larger content of cation in zeolite NaX, in our opinion. The sodium cation plays the important role

Table 2
The results of the NO_2-TPD experiments on the zeolites and other porous materials (all of the adsorbents were saturated with moisture at ambient temperature prior to adsorption of NO_2)

	NaY	NaY(a)[a]	NaX	Naβ	Hβ	MCM-48 -like	Activated carbon
Total amount ($\mu mol\,g^{-1}$)							
NO_2	373.6	301.4	669.4	263.1	67.6	53.3	759.3
NO_y[b]	28.37	NM	38.36	NM	27.08	NM	17.15
$NO_2(A)$[c] ($\mu mol\,g^{-1}$)	222.6	158.2	322.9	103.0	29.75	38.6	744.3
$NO_2(B)$[d] ($\mu mol\,g^{-1}$)	151.0	143.2	346.5	160.1	37.86	14.7	15.0
Total amount ($\mu mol\,m^{-2}$)	0.488	0.393	0.744	0.441	0.111	0.059	0.759
T_{max} (K)	573	613	773	673	493	413	433

NM: not measured.

[a] This sample was activated prior to adsorption.

[b] Reduced NO_2.

[c] Desorption before 773 K.

[d] Desorption after 773 K.

in the adsorption of NO_2, probably through electrostatic interaction to attract the adsorbate. Judged on the Si/Al ratio of zeolite, NaX has the lowest Si/Al ratio and the largest Al content and of course the largest amount of cation. These cations certainly exert the attraction on the NO adsorbates, holding them harder therefore some of them cannot desorb until the temperature achieves 773 K plus the purge of carrier gas.

The mesoporous silica with MCM-48 structure only adsorbed 53.3 $\mu mol\,g^{-1}$ NO_2 and furthermore ca. 72% then desorbed during calefactive stage (Table 2), though this sample had a larger pore size and higher surface area than NaY zeolites. One reason to cause this difference, in our opinion, is the presence of cation in zeolite. For example, the cation density of NaX was higher than NaY due to the lower Si/Al ratio [21] and MCM-48 had no cation in its siliceous composition. On the other hand, comparison of Naβ against Hβ revealed the impact of surface acidic–basicity on the adsorption of NO_2. The proton in Hβ seemed to reduce the NO_2 desorption (26.3 $\mu mol\,g^{-1}$), much lower than its basic analogue Naβ.

Nonetheless, these porous samples have different surface area hence the collision possibility of adsorbate–adsorbent that leads to successful adsorption will be different. To exclude the effect of surface area on the actual adsorption of the sample, the results shown in Table 2 are conversed to $\mu mol\,m^{-2}$. The amount of NO_2 desorbed was 0.744 $\mu mol\,m^{-2}$ for NaX, higher than the other zeolites and MCM-48-like but close to activated carbon (0.759 $\mu mol\,m^{-2}$).

As previously reported on thermally activated zeolites [19], the adsorbed NO_2 was reduced at high temperature to other nitrogen oxides (NO, N_2O_3 or N_2O, combined as NO_y). This was different on the moisture-saturated adsorbents in this study (with the exception of Hβ), as most of the desorbed nitrogen oxides were still present as NO_2 and only about 2% (activated carbon) and 7% of NO_2 were reduced to NO_y.

Fig. 1 delineates the NO_2 desorption curves on three zeolites with similar pore size and on two other materials as measured by TPD (the dashed line shows the temperature program). Apart from two small peaks around 353 and 413 K, the main desorption peak appeared around 573 K for NaY at ca. 87.8 $\mu mol\,g^{-1}$ of NO_2, accompanied by a shoulder at 713 K. There were three desorption peaks for NaX: a very weak peak at 373 K, a main peak at 773 K and a broad peak from 613 to 673 K. For Naβ, the maximum of NO_2 desorption appeared at 673 K together with a weak peak around 473 K. The lowest desorption peak was observed on the MCM-48-like at 413 K. Activated carbon was an efficient reversible adsorbent for NO_2 and most of the NO_2 desorbed near 433 K. In other words, the zeolites such as NaX adsorbed NO_2 much stronger than activated carbon under elevated temperature.

Fig. 2 depicts the effects of CuO loading in NaY on the NO_2 adsorption. A much higher adsorption capacity emerged on the modified NaY, indicating the interaction between the CuO added and NO_2. This contrasted with the fact that CuO itself could hardly absorb NO_2 because of its small surface area. Dispersion of CuO on zeolite NaY significantly enhanced the adsorption, resulting in a shift for the main desorption peak from about 573 K to above 670 K (Fig. 2A). When the CuO loading was increased from 1%CuO/NaY to 3%CuO/NaY and finally to 5%CuO/NaY, an incremental increase for the amount of NO_2 was detected, from 516 to 593 and finally to 813 $\mu mol\,g^{-1}$. However, further addition of CuO on NaY reduced the amount of NO_2 desorbed. For example, at 10% (w/w) CuO, only
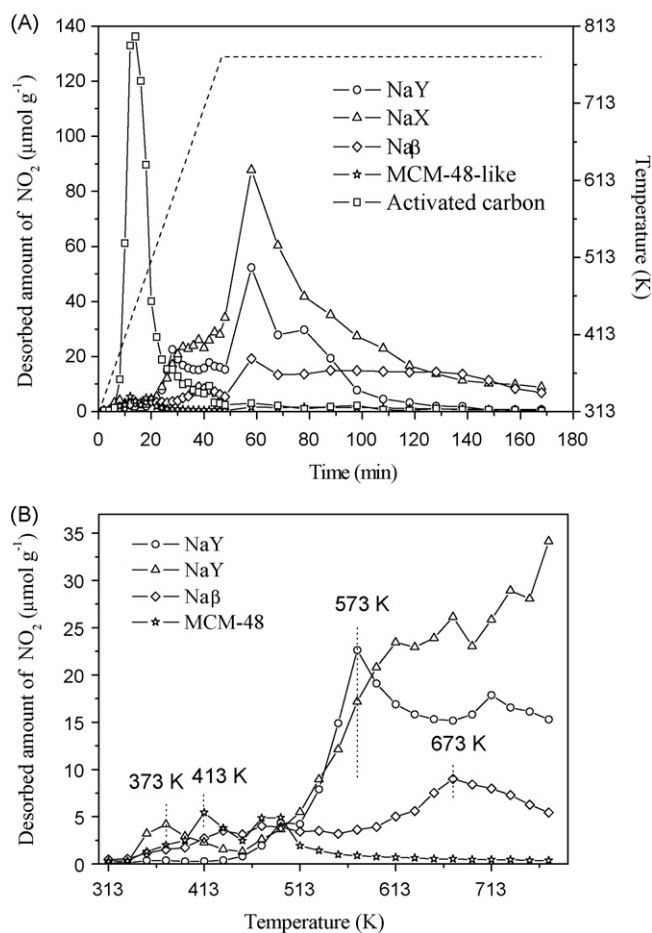

Fig. 1. TPD curves of NO_2 (A) on zeolite NaY, NaX, Naβ and MCM-48-like composite as well as activated carbon samples; (B) on zeolite NaY, NaX, Naβ and MCM-48-like composite before 773 K.
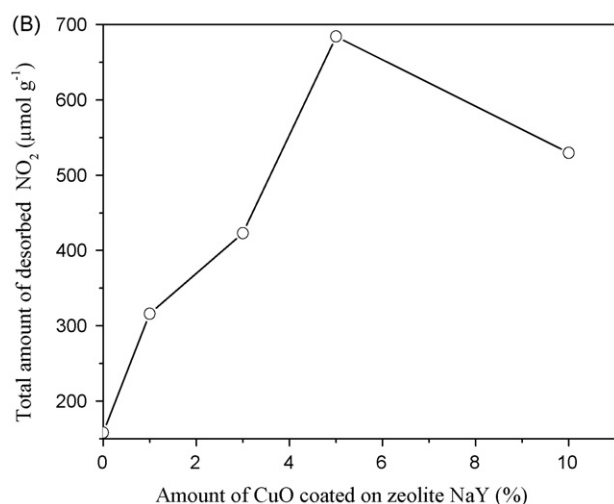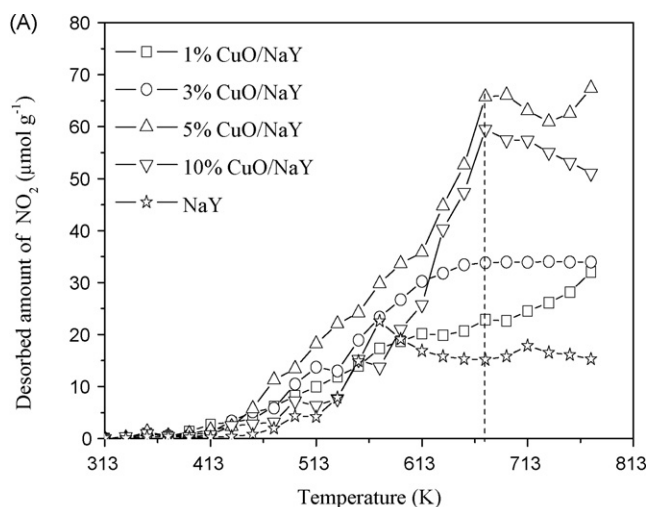
Fig. 2. (A) The TPD profile of NO_2 desorbed before 773 K from copper-modified NaY and (B) the influence of coating copper on the desorption of NO_2 before 773 K (all of these samples were activated at 773 K prior to adsorption of NO_2).

Fig. 3. The influence of the adsorption manner of NO_2 on the desorption of NO_2 from NaY zeolite in the procedure of TPD.

ion exchange hence their adsorption behaviors are different. As seen in Fig. 2A, dispersion of CuO on zeolite NaY significantly enhanced the adsorption, resulting in a shift for the main desorption peak from 573 K to above 670 K, while the amount of desorbed of NO_2 gently increased as the temperature rose from 413 to 673 K. Although exchanged copper cation also made the maximum desorption temperature of CuY-n shifted to high temperature (Fig. 4), the peak position shifted to relatively lower temperature as the ion exchange times increased. And from the climax peak to 773 K, the amount of desorbed NO_2 declined much quickly than that in the impregnated sample so that another peak seemed to appear. Besides, desorption of NO_2 from the exchanged sample was much quickly than that from impregnated sample, especially in the range of 443–613 K, forming the climax before 663 K. These differences resulted from the different total number of cation in two series of sample. Exchange of zeolite NaY with Cu^{2+} ion reduced the absolute number of the cation while the total number of cation in the copper-impregnation sample was increased. Since the number of cation in zeolites took charge in attracting NO_2 so that the CuY-n sample possessed the adsorption peak at the lower temperature than the CuO-incorporated samples. Likewise, stronger interaction and blocked channel caused by the more cations in the

$617\ \mu mol\ g^{-1}$ of NO_2 desorption was measured (Fig. 2B). In summary, loading 3–5% CuO on NaY was beneficial to enhance the NO_2 adsorption and further increase in CuO loading would have a negative impact on the adsorption.

Fig. 3 compares the amount and the profile of NO_2 desorbed on 5%CuO/NaY under the static and the dynamic adsorption methods. The results indicate that the modified NaY had virtually the same adsorption capacity under the two test methods. Despite the short residence time, ca. 0.6 s, the 5%CuO/NaY composite was still able to capture NO_2 in the gas flow. Similar to the other moisture-saturated adsorbents, this composite also exhibited a low tendency to deoxidize NO_2, only ca. 3% was converted to NO_y.

Fig. 4 exhibits the effects of the multiple exchanges with Cu^{2+} on NaY. The amount of NO_2 desorbed was 734, 739 and 795 $\mu mol\ g^{-1}$, respectively, from the sample exchanged 1, 2 and 3 times. These values were higher than that of 3%CuO/NaY but lower than 5%CuO/NaY. With increase in the exchange steps, the main peak temperature was shifted from 693 to 633 K (Fig. 4). Overall, multiple exchange with Cu^{2+} had no further improvement on the adsorption and the final product was inferior to 5%CuO/NaY. Comparing Figs. 2A and 4 can reveal the different property-function ration of the copper-modified NaY zeolite prepared by two methods, in which one sample is prepared through impregnation and another through
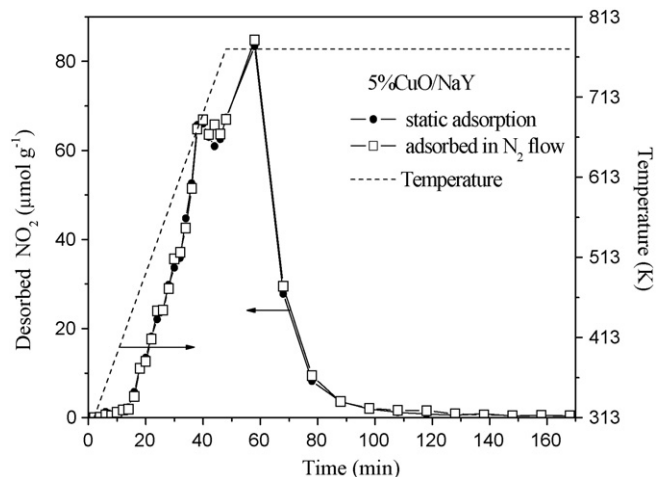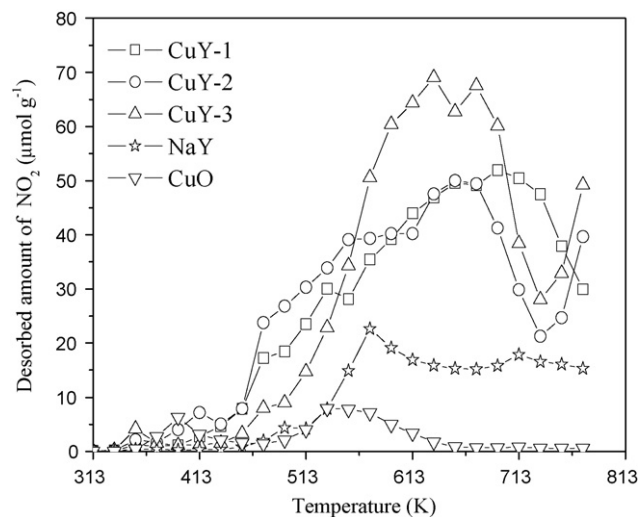

Fig. 4. TPD curves of NO_2 from the zeolite NaY exchanged by Cu^{2+} with different times before 773 K.
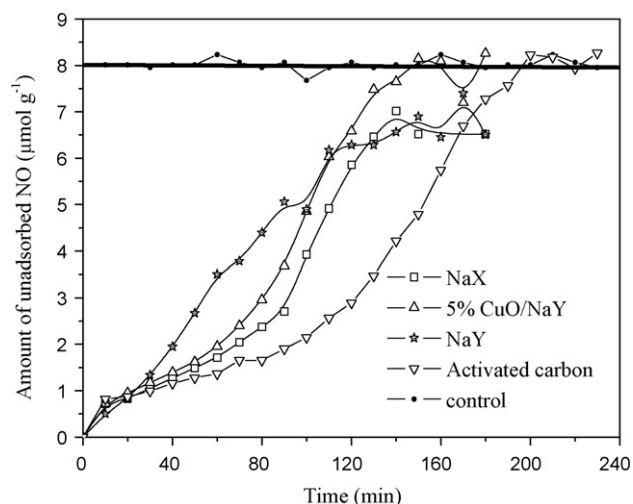
Fig. 5. Instantaneous adsorption of NO on NaY, NaX, 5%CuO/NaY and activated carbon samples at 303 K.

copper-incorporated sample made desorption of NO_2 difficult therefore the amount of NO_2 detected after the peak climax still keep high.

3.2. Instantaneous adsorption of NO on zeolites

NO existed in fresh cigarette smoke as the main nitrogen oxide therefore its adsorption by moisture-saturated zeolites was evaluated by the instantaneous adsorption method and Fig. 5 illustrates the results in which the solid horizontal line is the concentration of NO in the original gas mixture. One of the blank results was also shown to demonstrate that no loss of NO occurred without the adsorbent. The profiles show that the adsorption by the zeolite was gradual and the amount of residual NO in the gas stream increased as the adsorption continued. The ranking in adsorption capacity was: NaX > 5%CuO/NaY > NaY. The full adsorption for NO is 67.7, 61.8 and 59.6 $\mu mol\,g^{-1}$, reached after about 3 h with corresponding adsorption ratio at 53.1, 43.2 and 42.9%, respectively. Activated carbon exhibited a higher adsorption than NaX (Fig. 5) and it captured 96.4 $\mu mol\,g^{-1}$ of NO at 3 h, corresponding to 66.9% adsorption ratio.

Fig. 6 presents the results from the instantaneous adsorption tests on NaX under different flow rates. At 15 ml min^{-1}, it took ca. 270 min for NaX to reach its saturation level. A total of 118 $\mu mol\,g^{-1}$ of NO passed through the material and 68.3% was adsorbed. As the flow rate increased to 60 ml min^{-1}, the adsorption capacity of the sample decreased to ca. 15.6 $\mu mol\,g^{-1}$ (Fig. 6A). In addition, the change of flow rate had a significant effect on the breakthrough curve, the larger the flow rate was, the faster saturation of the NO reached with a higher slope. These facts suggest a mass transfer limited mechanism for NO adsorption, which differed from the adsorption of volatile nitrosamines by NaY that was relatively independent of the gas flow rate [23]. In general, the slower flow rate led to the larger contact time between the NO and zeolite NaX, which was beneficial for the adsorption (Fig. 6B). At 15 ml min^{-1}, the contact time between NO and NaX was ca. 0.5 s. As the flow rate rose to 60 ml min^{-1}, the contact time was reduced to ca. 0.1 s and was comparable to that experienced by an adsorbent in a cigarette filter consequently NaX maintained about one-sixth of its ability to capture NO (Fig. 6B). Under this flow rate, however, the sample of NaX could adsorb NO again after the achievement of maximum at 50th min, which probably related to formation of adsorbed $(NO)_2$ dimers [31–33]. When the concentration of strong adsorbed NO
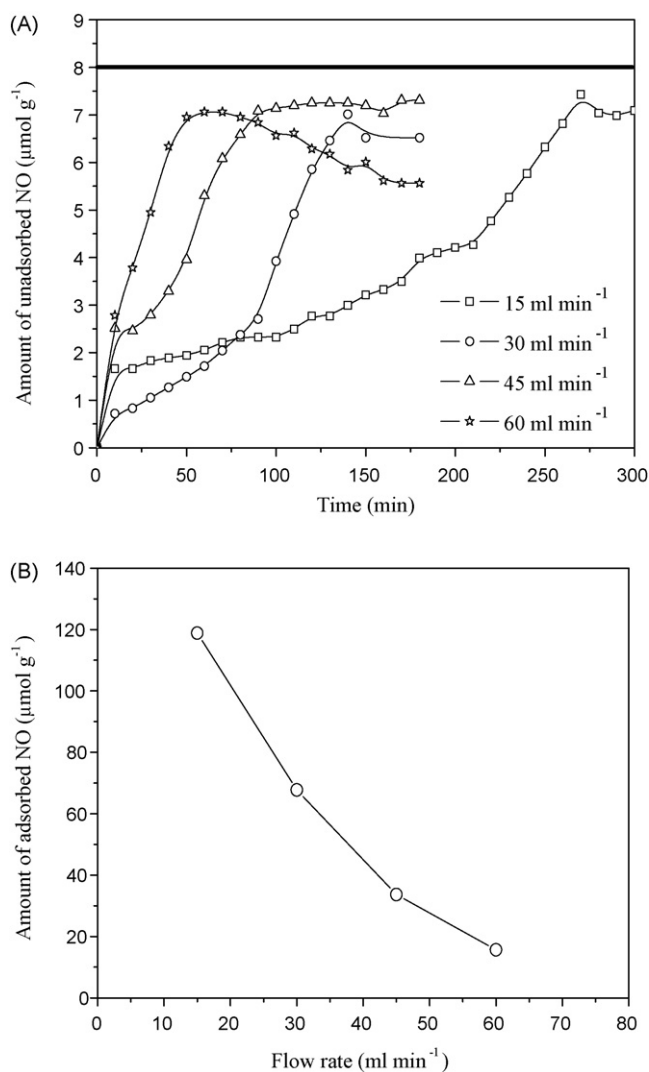

Fig. 6. (A) Instantaneous adsorption of NO on NaX with different flow rate and (B) the effect of flow rate of carrier gas on the adsorption of NO by zeolite NaX saturated with moisture at 303 K.

was high, two NO molecules adjacent located could form an $(NO)_2$ dimer, which enabled the adsorptive sites to be liberated hence they would adsorb new NO molecules again. In our opinion, the formation of dimer needs time and suitable condition, probably the enough amount of adsorbed NO. The high speed of carrier gas enabled the adsorbed NO to be diffused quickly so that the formation of dimer was promoted. As the result, after the sample reached its maximum adsorption capacity at 50th min, the new adsorbed NO spurred the formation of dimer and the adsorbent began to adsorb again. However, further investigation is desirable for understanding this phenomenon.

As described in the introduction, cigarette smoke contains many volatile and condensed phase compounds that may hinder the NO_x adsorption by zeolites. In a simple test to assess the impact of organic compounds on the NO adsorption, NaX was pre-adsorbed with benzene, acetaldehyde and 1,3-butadiene and tested for their instantaneous adsorption capability. These compounds were chosen because they were known smoke toxicants and were present at relatively higher levels [10]. As is evident in Fig. 7, the material with pre-adsorbed benzene appeared to have a higher NO adsorption, a total of 101 $\mu mol\,g^{-1}$ or 75%. Similar effects were also observed in the sample with pre-adsorbed acetaldehyde. Benzene
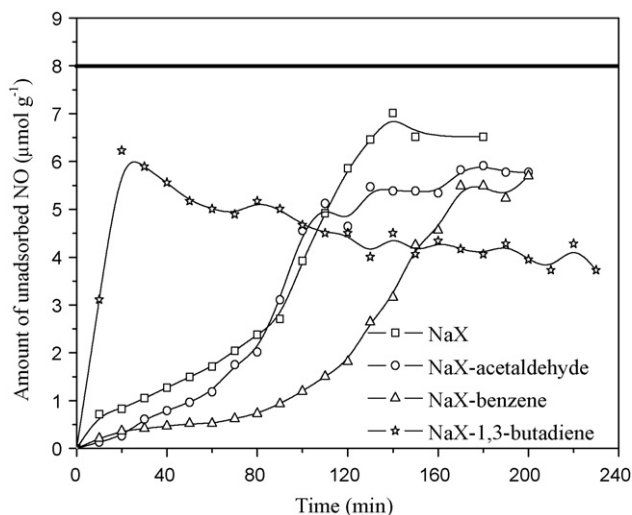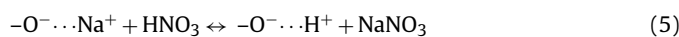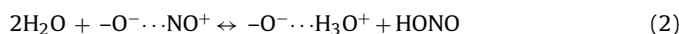
Fig. 7. The effect of pre-adsorbed organic compounds on the adsorption of NO by zeolite NaX saturated with moisture at 303 K.

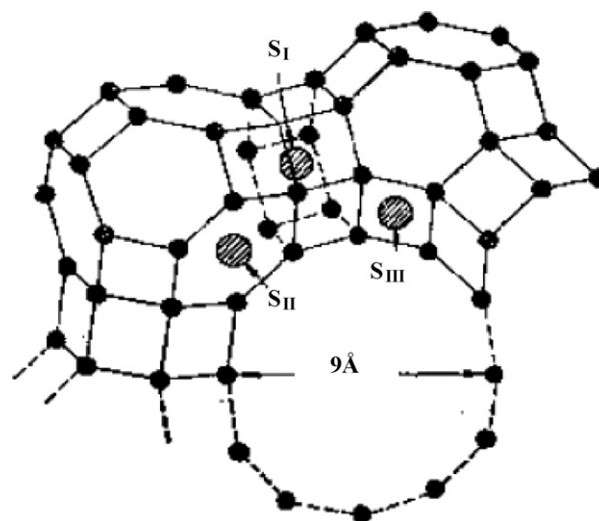**Scheme 1.** The structure of Faujasite-type zeolite and cation locations [21].

was bound to zeolites via π-bonding mechanism, and it might act as π-donor while the adsorbed NO being the electron acceptor [34,35]. A similar interaction between NO and acetaldehyde was observed on NaY [36], and the reaction responsible for the interaction was proposed to be [37]: $CH_3CHO + NO_3^- \rightarrow CH_3COOH + NO_2$ and/or $CH_3COO^- + H^+NO_2^-$. However, the NaX with pre-adsorbed 1,3-butadiene reached its saturation quickly and then the adsorption continued with exposure time. Formation of organic nitrogen-containing intermediates through the interaction of the adsorbed NO with hydrocarbon species has been reported before [38]. This may be counter-balanced by the competitive adsorption between the organics and NO for the same adsorptive site [39,40]. The exact mechanism by which pre-adsorbed organics interact with the subsequent absorption remained to be investigated.

4. Discussion

For the zeolites investigated, the results obtained in this work show that they still maintained relatively high adsorption for NO_2 even in the presence of water. However, the zeolite–water combination generated different adsorbed NO_x species, and this observation agreed with a previous study on the adsorption of NO_2 over Na- and Ba-Y [36,41]. The reaction between NO_2 and H_2O in the channels of NaY might follow these different steps depending on the amount of adsorbed water [36,41],

$$2NO_2 \leftrightarrow NO^+ + NO_3^- \tag{1}$$

$$2H_2O + -O^-\cdots NO^+ \leftrightarrow -O^-\cdots H_3O^+ + HONO \tag{2}$$

$$3NO_2 + H_2O \leftrightarrow 2HNO_3 + NO \tag{3}$$

$$2NO_2 + H_2O \leftrightarrow HNO_3 + HONO \tag{4}$$

$$-O^-\cdots Na^+ + HNO_3 \leftrightarrow -O^-\cdots H^+ + NaNO_3 \tag{5}$$

If zeolite contained water prior to NO_2 adsorption, a signature presence of NO_3^- and NO_2^- was expected. With increasing amount of water, there was greater amount of NO_2^- being produced. The HNO_3 thus formed quickly interacts with the charge-compensating ions (e.g., Na^+) to create Brönsted acidic sites and Na-nitrates. These species were stable on wet NaY and upon heating desorb as NO_2 at temperatures higher than 500 K. This matched relatively well with the peak temperatures of 573 and 773 K as observed in this work. The high temperature of NO_2 desorption peaks are always accompanied by water desorption, which strongly suggests that NO_2 is

formed in the reverse of reaction step (4), i.e., both HNO_3 and HONO decompose to form NO_2 and water.

Compared to NaY, the broader peak for NaX (from 613 to 673 K) may be explained by the fact that NaX possesses more sites to interact with NO_2. The enhanced NO_2 adsorption led to the higher NO_2 desorption temperature. Also, the 773 K NO_2 desorption peak may be related to the formation of nitrate species, as shown by Szanyi et al. [36].

For Faujasite-type zeolites like NaY and NaX, their different adsorption for NO_2 indicates that cationic sites are primarily responsible for NO_2 adsorption. Na ions in the S_I-sites of X- and Y-type zeolites are not accessible to NO_2 molecules because the entrance of the hexagonal prism ($\sim$0.22 nm, Scheme 1) is smaller than the molecular diameter of NO_2 (0.346 nm) [21], therefore it is the Na^+ cations on the S_{II} and S_{III} positions contributed to NO_2 adsorption. The ratio of Na^+ cations on S_{II} and S_{III} for NaX and NaY is 1.75 [21] and the higher ratio is mainly caused by a higher S_{III} number, as the numbers of the cations on S_{II} are the same for NaX and NaY (i.e., 32). As a result, the amount of NO_2 detected from NaX in our TPD experiments was 0.79-fold higher than that from NaY. NaX has more cations than the MCM-48-like mesoporous silica and the other zeolites studied here. The fact that they all showed inferior adsorption than NaX confirms the important role-played by the cation in the adsorption of NO_2. Furthermore, it was calculated that the ratio of adsorbed NO_2 to Na^+ ion was about 1:6 in zeolite NaX while on zeolite NaY this value was about 1:8. The other factor contributing to NaX's performance for the adsorption of NO_2 is its strong hydrophilicity due to its higher aluminum [21]. As discussed before, the presence of water promotes the adsorption of NO_2.

The results shown in Figs. 2 and 3 reveal that incorporating copper to form composites can enhance the zeolite's inherent adsorption for NO_2. However, the optimum adsorption was established by coating NaY with 5%CuO and no more (Fig. 2B). We have found that aggregation of CuO occurred when the CuO loading reached ca. 10% (w/w) by monitoring XRD spectra from the prepared samples [26], indicating that the dispersion of copper guest in NaY could no longer be maintained at this high loading. The aggregated CuO caused worsening adsorption by obstructing the channels of NaY and reducing the surface area and pore volume [26]. The surface area was reduced from 766 m^2 g^{-1} (NaY) to 501 m^2 g^{-1} (10%CuO/NaY), while the pore volume decreased by about 13%.

It is possible that the presence of aggregated CuO changed the previous reactions to form the nitrate species [42]. For example, the adsorbed NO_2 may be stored as

$$3NO_2 + [CuO] \rightarrow NO + Cu(NO_3)_2 \qquad (6)$$
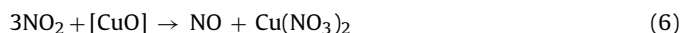
Finally it is possible to open up the N–O bond scission on CuO/NaY and to release NO_2 in the desorption steps:

$$Cu(NO_3)_2 \rightarrow 2NO_2 + [CuO] + (1/2)O_2 \qquad (7)$$

$$Cu(NO_3)_2 + NO \rightarrow 3NO_2 + [CuO] \qquad (8)$$
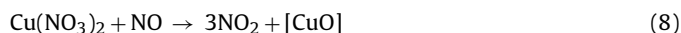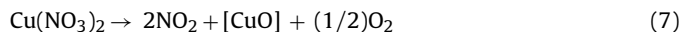
The high reactivity of NO with nitrates at low temperatures has a strong influence on the stability of the nitrates formed during the adsorption of NO_2 [42]. As a result, the NO_2 and its derivatives may be held more tightly on the CuO modified samples.

The composition of NaY ($Na_{49}[(AlO)_{49}(SiO)_{140}]\cdot 268H_2O$) has a sodium content of ca. 8.29% (w/w). For ion exchange, one Cu^{2+} cation replaces two Na^+ cations in the zeolite:

$$2Na^+(zeolite) + Cu^{2+}(aq) \leftrightarrow Cu^{2+}(zeolite) + 2Na^+(aq) \qquad (9)$$
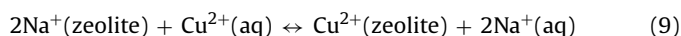
Consequently a fully exchanged CuY should have ca. 11.2% (w/w) of copper. Due to the geometric limitation, the Na^+ ions located in the S_I and S_{II} positions of NaY (Scheme 1) can be more easily replaced than those in the S_{III} position. This led to a fraction of the Na^+ ions in NaY being replaced by Cu^{2+} during the first exchange and both Cu^{2+} and Na^+ cations co-existed in the sample.

Repeating the exchange procedure incorporated more Cu^{2+} ions into the zeolite framework. However, the Cu^{2+} ions exchanged could not enter the S_{III} position [43] and those in the S_I-sites were not accessible to NO_2 molecules [21,44], hence the CuY-2 and CuY-3 displayed similar adsorption capacity as to CuY-1, and the ratio of adsorbed NO_2 molecule to copper ions was about 1:2.

Upon adsorbing NO_2, NO^+ and NO_3^- are formed in disproportion to NO_2: $2NO_2 \leftrightarrow NO^+ + NO_3^-$. The NO^+ binds to an O^- site on the zeolite framework, replacing a Na^+ ion, while the NO_3^- binds to a Na^+ ion [36]. Since some Na^+ ions in NaY could not interact with these nitrogen oxides owing to the space limitation, the coverage of cationic sites by the adsorption of NO_2 usually reached ca. 41% [27]. Exchange of NaY with Cu^{2+} ions therefore lowered the number of cations but enhanced their accessibility, and this promoted the adsorption of NO_2 on CuY (Fig. 4).

On the other hand, the impregnation of NaY with copper oxide (i.e., not the ion exchange method) had its drawback because the added CuO could obstruct the channels of NaY. The overall effect of the impregnation on the adsorption was thus inferior to that of the ion exchange. In summary, the different behaviors of the copper-containing NaY prepared by the impregnation and the ion exchange are the results of a complex balance between the electrostatic interaction and the geometric confinement.

5. Conclusion

The zeolites with large micropores were able to adsorb significant amounts of NO_2 even when they were saturated with water, which is valuable for environment protection. Among the zeolites investigated, NaX exhibited a higher capability than NaY in the adsorption of nitrogen oxides, because of its higher cation numbers and stronger hydrophilicity.

Introducing controlled levels of copper into NaY zeolite through either impregnation or ion exchange promoted the adsorption towards NO_2 or NO, due to the strengthened electrostatic interaction toward the adsorbates. Pre-adsorbed organics displayed complex adsorption behavior, some accelerate while some cumber the adsorption of NO by zeolite NaX, which depended on the organic and the interaction with NO and the zeolite substrate. The

adsorption of NO_2 on Faujasite demonstrated potentials to use these materials to remove nitrogen oxides in treating polluted gas streams.

Appendix A. Supplementary data

Supplementary data associated with this article can be found, in the online version, at doi:10.1016/j.jhazmat.2008.05.111.

References

[1] V.I. Pârvulescu, P. Grange, B. Delmon, Removal of NO, Catal. Today 46 (1998) 233–316.
[2] M. Shelef, Selective catalytic reduction of NOx with N-free reductants, Chem. Rev. 95 (1995) 209–225.
[3] M.A. Hess, M.J. Haas, T.A. Foglia, W.N. Marmer, The effect of antioxidant addition on NOx emissions from biodiesel, Energy Fuels 19 (2005) 1749–1754.
[4] I.V. Babich, K. Seshan, L. Lefferts, Nature of nitrogen specie in coke and their role in NO_x formation during FCC catalyst regeneration, Appl. Catal. B 59 (2005) 205–211.
[5] V.G. Komvokis, E.F. Iliopoulou, I.A. Vasalos, K.S. Triantafyllidis, C.L. Marshall, Development of optimized Cu–ZSM-5 deNOx catalytic materials both for HC-SCR applications and as FCC catalytic additives, Appl. Catal. A 325 (2007) 345–352.
[6] G. Qi, R.T. Yang, Ultra-active Fe/ZSM-5 catalyst for selective catalytic reduction of nitric oxide with ammonia, Appl. Catal. B 60 (2005) 13–22.
[7] H. Bosch, F. Jansen, Formation and control of nitrogen oxides, Catal. Today 2 (1988) 369–379.
[8] V. Norman, A.M. Ihrig, T.M. Larsen, B.L. Moss, The effect of some nitrogeneous blend components on NO/NOx and HCN levels in mainstream and sidestream smoke, Beitr. Tabakforsch. Inernat. 12 (1983) 55–62.
[9] R.A. Jenkins, B.E. Gill, Determination of oxides of nitrogen (NOx) in cigarette smoke by chemiluminescent analysis, Anal. Chem. 52 (1980) 925–928.
[10] R.R. Baker, in: D.L. Davis, M.T. Nielsen (Eds.), Tobacco Production, Chemistry, and Technology, Blackwell Science, London, 1999, pp. 412–413.
[11] D. Hoffmann, I. Hoffmann, The changing cigarette, 1950–1995, J. Toxicol. Environ. Health 50 (1997) 307–364.
[12] International Agency for Research on Cancer (IARC), Chemistry and analysis of tobacco smoke, in: IARC Monograph on the Evaluation of the Carcinogenic Risk of Chemicals to Humans. Tobacco Smoking, IARC, Lyon, 1985, vol. 38, pp. 83–126.
[13] R.M. Estefan, E.M. Gause, J.R. Rowlands, Electron spin resonance and optical studies of the interaction between NO_2 and unsaturated lipid components, Environ. Res. 3 (1970) 62–87.
[14] B. Shen, L.L. Ma, J.H. Zhu, Q.H. Xu, Decomposition of N-nitrosamines over zeolites, Chem. Lett. (2000) 380–381.
[15] W.C. Matthews, H.C. Shaw, Selective adsorption of nitrogen oxides, U.S. Patent 4,153,429, assigned to Union Carbide Corporation, USA (1979).
[16] J.A. Sullivan, O. Keane, A combination of NOx trapping materials and urea-SCR catalysts for use in the removal of NO_x from mobile diesel engines, Appl. Catal. B 70 (2007) 205–214.
[17] S. Van Roosbroeck, J. Wichmann, N.A.H. Janssen, G. Hoek, J.H. Wijnen, E. Lebret, B. Brunekreef, Long-term personal exposure to traffic-related air pollution among school children, a validation study, Sci. Total Environ. 368 (2006) 565–573.
[18] J.H. Zhu, S.L. Zhou, Y. Xu, Y. Cao, Y.L. Wei, Ordered mesoporous materials. Novel catalyst for degradation of N′-nitrosonornicotine, Chem. Lett. 32 (2003) 338–339.
[19] Y. Xu, J.H. Zhu, L.L. Ma, A. Ji, Y.L. Wei, X.Y. Shang, Removing nitrosamines from mainstream smoke of cigarettes by zeolites, Micropor. Mesopor. Mater. 60 (2003) 125–138.
[20] W.M. Meier, K. Siegmann, Significant reduction of carcinogenic compounds in tobacco smoke by the use of zeolite catalysts, Micropor. Mesopor. Mater. 33 (1999) 307–364.
[21] D.W. Breck, Zeolite Molecular Sieves, Wiley-Intersciences, New York, 1974.
[22] J.H. Zhu, Y. Chun, Q.H. Xu, Y. Qin, Novel porous material derived from hydrolysis of aluminum isopropoxide on NaY zeolite, Mater. Lett. 33 (1998) 331–335.

[23] C.F. Zhou, Y. Cao, T.T. Zhuang, W. Huang, J.H. Zhu, Capturing volatile nitrosamines in gas stream by zeolites: why and how, J. Phys. Chem. C 111 (2007) 4347–4357.
[24] S. Bennici, A. Gervasini, N. Ravasio, F. Zaccheria, Optimization of tailoring of CuOx species of silica alumina supported catalysts for the selective catalytic reduction of NOx, J. Phys. Chem. B 107 (2003) 5168–5176.
[25] H. Yahiro, M. Iwamoto, Copper ion-exchanged zeolite catalysts in deNOx reaction, Appl. Catal. A 222 (2001) 163–181.
[26] Y. Xu, H.D. Liu, J.H. Zhu, Z.Y. Yun, J.H. Xu, Y. Cao, Y.L. Wei, Removal of volatile nitrosamines with copper modified zeolites, New J. Chem. 28 (2004) 244–252.
[27] Z.M. Wang, T. Arai, M. Kumagai, Adsorption separation of low concentrations of CO_2 and NO_2 by synthetic zeolites, Energy Fuels 12 (1998) 1055–1060.
[28] C.F. Zhou, J.H. Zhu, Adsorption of nitrosamines in acidic solution by zeolites, Chemosphere 58 (2005) 109–114.
[29] C.F. Zhou, Y.M. Wang, T.T. Zhuang, Y. Wang, J.H. Zhu, New efficient Al-containing SBA-15 materials for removing nitrosamines in mild conditions, Stud. Surf. Sci. Catal. 156 (2005) 907–916.
[30] Z.Y. Wu, Y.M. Wang, W.W. Huang, J. Yang, H.J. Wang, J.H. Xu, Y.L. Wei, J.H. Zhu, Formation of cubic $Ia3d$ silicas and metal oxide-loaded silicas using a triblock copolymer ($EO_{20}PO_{70}EO_{20}$)-acetate mixture as structure director in aqueous solution, Chem. Mater. 19 (2007) 1613–1625.
[31] O. Byl, P. Kondratyuk, J.T. Yates, Adsorption and dimerization of NO inside single-walled carbon nanotubes—an infrared spectroscopic study, J. Phys. Chem. B 107 (2003) 4277.
[32] W. Klose, S. Rincón, Adsorption and reaction of NO on activated carbon in the presence of oxygen and water vapour, Fuel 86 (2007) 203–209.
[33] R.Q. Long, R.T. Yang, Carbon nanotubes as a superior sorbent for nitrogen oxides, Ind. Eng. Chem. Res. 40 (2001) 4288–4291.
[34] M. Stichler, R. Weimar, D. Menzel, The influence of electronegative coadsorbates on the geometry of benzene on Ru(0 0 1), Surf. Sci. 384 (1997) 179–191.
[35] P.V. Jasen, E.A. Gonzalez, A. Juan, G. Brizuela, Benzene and NO on a Ru(0 0 1) surface: electronic structure and bonding, Appl. Surf. Sci. 252 (2006) 2108–2114.
[36] J. Szanyi, J.H. Kwak, R.A. Moline, C.H.F. Peden, The adsorption of NO_2 and the $NO^+O_2^-$ reaction on Na-Y, FAU: an in situ FTIR investigation, Phys. Chem. Chem. Phys. 5 (2003) 4045–4051.
[37] J. Szanyi, J.H. Kwak, R.A. Moline, C.H.F. Peden, Adsorption, coadsorption, and reaction of acetaldehyde and NO_2 on Na-Y, FAU: an in situ FTIR investigation, J. Phys. Chem. B 108 (2004) 17050–17058.
[38] S.J. Schmieg, B.K. Cho, S.H. Oh, Selective catalytic reduction of nitric oxide with acetaldehyde over NaY zeolite catalyst in lean exhaust feed, Appl. Catal. B 49 (2004) 113–125.
[39] T.P. O'Connor, J. Mueller, Modeling competitive adsorption of chlorinated volatile organic compounds with the Dubinin–Radushkevich equation, Micropor. Mesopor. Mater. 46 (2001) 341–349.
[40] Y. Takeuchi, H. Iwamoto, N. Miyata, S. Asano, M. Harada, Adsorption of 1-butanol and p-xylene vapor and their mixtures with high silica zeolites, Sep. Technol. 5 (1995) 23–34.
[41] J. Szanyi, J.H. Kwak, C.H.F. Peden, The effect of water on the adsorption of NO_2 in Na- and Ba-Y, FAU zeolites: a combined FTIR and TPD investigation, J. Phys. Chem. B 108 (2004) 3746–3753.
[42] J. Despres, M. Koebel, O. Kröcher, M. Elsener, A. Wokaun, Adsorption and desorption of NO and NO_2 on Cu-ZSM-5, Micropor. Mesopor. Mater. 58 (2003) 175–183.
[43] A.A. Verberckmoes, B.M. Weckhuysen, J. Pelgrims, R.A. Schoonheydt, Diffuse reflectance spectroscopy of dehydrated cobalt-exchanged Faujasite-type zeolites: a new method for Co^{2+} siting, J. Phys. Chem. 99 (1995) 15222–15228.
[44] P. Concepción-Heydorn, C. Jia, D. Herein, N. Pfänder, H.G. Karge, F.C. Jentoft, Structural and catalytic properties of sodium and cesium exchanged X and Y zeolites, and germanium-substituted X zeolite, J. Mol. Catal. A: Chem. 162 (2000) 227–246.